Structural changes with lead substitution in $Bi_{2-x}Pb_xSr_2CoO_6$

2000 J. Phys.: Condens. Matter 12 5371

(http://iopscience.iop.org/0953-8984/12/25/303)

J. Phys.: Condens. Matter **12** (2000) 5371–5389. Printed in the UK PII: S0953-8984(00)09483-2

Structural changes with lead substitution in $Bi_{2-x}Pb_xSr_2CoO_6$

N Jakubowicz, D Grebille†, M Hervieu, H Leligny and B Raveau
Laboratoire CRISMAT (UMR CNRS 6508), ISMRA, 14050 Caen Cédex, France

Received 11 November 1999, in final form 9 March 2000

Abstract. Structures refined for two members of the group of $Bi_{2-x}Pb_xSr_2CoO_6$-type compounds are proposed. For $x = 0.16$, the structure is incommensurately modulated ($a = 5.453(2)$ Å, $b = 5.426(2)$ Å, $c = 23.43(1)$ Å, $\vec{q}^\star = 0.245(2)\vec{b}^\star + \vec{c}^\star$, $F2mm(0\beta1)00s$). For $x = 0.8$, the modulation becomes very weak and has been neglected in the structural refinement ($a = 5.3117(7)$ Å, $b = 5.4232(6)$ Å, $c = 23.590(2)$ Å, $Pnan$). A new interpretation of the undoped modulated $Bi_2Sr_2CoO_6$ phase is given. A new type of configuration for the [BiO] layers is confirmed and original modulation features are elucidated in comparison with the related superconducting cuprate phases.

1. Introduction

In a recent paper [1], an accurate structural description of the modulated $Bi_2Sr_2CoO_6$ phase, related to the $Bi_2Sr_2CuO_6$ superconducting phase, was proposed. Attention was particularly focused on the description of the [BiO] layers of these well known layered structures, as they seem to be partly responsible first for the modulated character of the structure and second for the physical properties of the 2201 or 2212 cuprate phases as potential charge reservoirs.

Very few studies concerning the (Bi, Pb)–Sr–Co–O system have been published. Only the so-called 2201 phase ($Bi_{2-x}Pb_xSr_2CoO_6$) could be isolated. The undoped phase ($x = 0$) exhibits an incommensurate structural modulation [1, 2] that has the modulation vector $0.24\vec{b}^\star + \vec{c}^\star$. Both previous studies agree on the disordered character of the oxygen configuration of the [BiO] layers and two different hypotheses were proposed to give an interpretation for this disorder [1]. Partially replacing Bi with Pb involves an evolution of the modulation vector. The irrational component varies from $0.24b^\star$ up to $0.25b^\star$ with increasing Pb content. A Pb-doped phase with $x = 0.16$ and $\vec{q}^\star = 0.245\vec{b}^\star + \vec{c}^\star$ has been synthesized and its structure is proposed in the present study. On further increasing the Pb ratio, one obtains a new phase, with the appearance, in the diffraction pattern, of two types of satellite reflection: the first ones reproducing the sequences of the previous ones with $\vec{q}_I^\star = 0.25\vec{b}^\star + \vec{c}^\star$ but the second ones without a rational component: $\vec{q}_{II}^\star = 0.25\vec{b}^\star$. This phase can be described as a fourfold superstructure of the average structure of the lead-free phase. Unfortunately, the quality of the samples was not such as to allow any valid structural refinement. Finally, as the substitution rate increases still further (x around 0.8), the intensity of the satellites becomes very weak and the modulation disappears. The structure can be approximated by a structural model based on the unit cell of the average structure of the modulated phase.

In the present paper, we describe the structural refinement of the mono-incommensurate Pb-doped compound ($x = 0.16$) and of the highly doped phase ($x = 0.8$). Comparisons

† Author to whom any correspondence should be addressed.

0953-8984/00/255371+19$30.00

between these doped phases and the undoped compound are made. Thanks to these two studies, we can show that there are important differences between cobaltites and cuprates, with the stabilization of a new [BiO] layer configuration. The results obtained with a non-modulated model confirm a common configuration with the modulated phases. These results are also confirmed by HREM observations.

2. Experimental procedure

Single crystals of $Bi_{2-x}Pb_xSr_2CoO_6$ were prepared from a mixture of oxides and carbonates (Bi_2O_3, PbO, $SrCO_3$ and Co_3O_4) in the molar ratios Bi:1.8:Pb:0.2:Sr:4:Co:3 and Bi:1.2:Pb:0.8:Sr:3:Co:2 for the modulated and the non-modulated phases respectively. These reagents were heated in air at 850 °C for 20 h, then at 1100 °C for 1 h, slowly cooled down at 1 °C h^{-1} to 900 °C and then rapidly cooled down to 25 °C. Monodomain single crystals were mechanically isolated from the solidified material for both preparations. The crystal quality was tested with a Weissenberg camera. A first estimation of the crystal parameters and symmetry could be made.

The first phase (crystal A) exhibits a structural modulation. A platelet crystal ($0.40 \times 0.08 \times 0.024$ mm^3) was mounted on an Enraf-Nonius CAD4 Diffractometer. Cell refinements using 25 reflections lead to the following parameters: $a = 5.453(2)$ Å, $b = 5.426(2)$ Å, $c = 23.43(1)$ Å. A least-squares refinement from the measured θ-values of 20 satellite reflections as well as a profile analysis of selected first- and second-order satellite reflections allowed us to confirm the incommensurate character of the modulation $\vec{q}^{\star} = 0.245(2)\vec{b}^{\star} + \vec{c}^{\star}$. Diffracted intensities were measured both on an Enraf-Nonius CAD4 diffractometer and on a STOE IPDS using Mo Kα radiation. A EDX analysis carried out on a SEM confirmed the presence of lead in the proportion $Bi_{1.84}Pb_{0.16}Sr_{2.2}CoO_y$. Furthermore, on Weissenberg photographs, no diffuse scattering could be detected, in contrast to the case for the undoped phase $Bi_2Sr_2CoO_6$. This result corroborates assertions of a role of lead in obtaining crystals of better quality.

The second phase (crystal B), richer in Pb, is characterized by the almost complete disappearance of satellite reflections on Weissenberg photographs. Electron diffraction patterns obtained by TEM (JEOL 200CX working at 200 kV) show the presence of weak satellite reflections with intensity varying over a large range from one area to another. One example of an [001] ED pattern with a system of weak satellite reflections is given in figure 1(a), where they are indicated by small white arrows around the $\overline{2}\overline{2}0$ reflection. The system of intense reflections reveals an F-type lattice. However, very weak additional spots (dark arrows in figure 1(a)) are commonly observed in the [001] ED patterns. The reconstruction of the reciprocal space showed that they are generated by a complex intergrowth of different variants along $\vec{c}^{\star}$. These streaky lines are clearly observed in the $[1\bar{1}0]$ ED pattern (figure 1(b)) and explain why the F-lattice conditions are violated. EDS nanoanalyses using a Kevex system were performed on this preparation and confirmed the high and homogeneous Pb substitution rate leading to the composition $Bi_{1.2}Pb_{0.8}Sr_2CoO_y$. High-resolution images were obtained using a TOPCON 002B microscope of resolution 0.18 nm. The volume occupied by these modulated zones (figure 2(a)) beside the non-modulated ones throughout the whole crystal is generally small and varies according to the sample. An enlargement of the image (figure 2(b)) clearly shows, in modulated zones (denoted by m), typical antiphase undulations of the layers of the incommensurate compound. In non-modulated areas, domains denoted by 1 exhibit a regular 2201 stacking with the double [BiO] layers spaced by 12 Å. However, retaining the 2201 stacking mode, variations of contrast are observed which affect one double [BiO] layer out of two in other areas denoted by 1, 2. These variations appear in this image in the

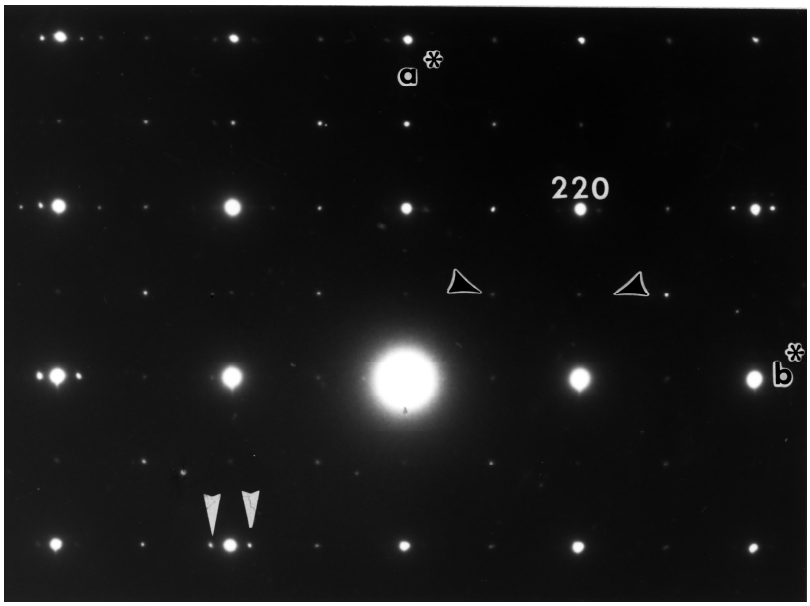

(a)

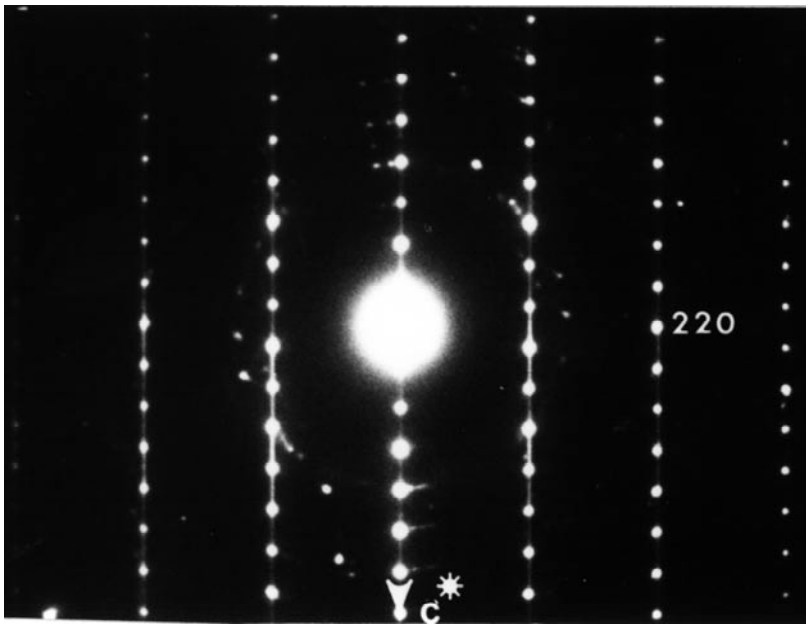

(b)

Figure 1. (a) An [001] ED pattern. Weak satellite reflections are indicated by white arrows. The dark arrows show weak reflections which violate the conditions of reflection and involve a P-type lattice. (b) A $[1\bar{1}0]$ ED pattern. The diffuse streaks along $\vec{c}^{\star}$ generate the P-type very weak spots in part (a).

form of dark or less dark areas at the level of the atomic rows running along $\vec{b}$, involving, for example in this zone, a real 24 Å periodicity. In other areas (denoted by i), more complex

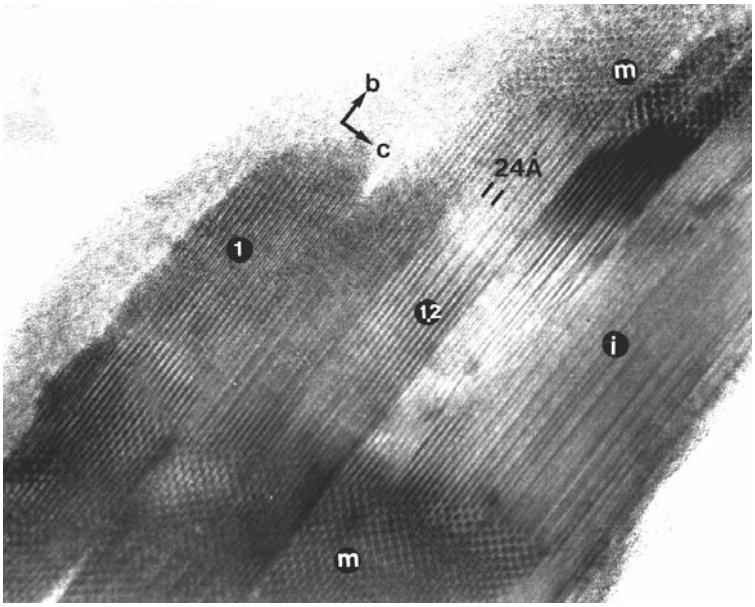

(a)

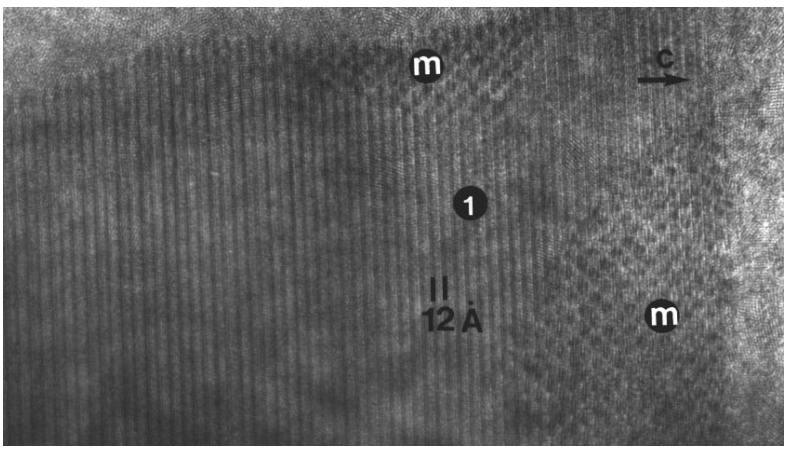

(b)

Figure 2. TEM images for highly doped crystals. These indicate the existence of modulated (called m) and non-modulated zones (called 1 or 1, 2). ((b) is an enlargement of part (a).)

sequences of the dark and grey rows are observed. This suggests that there are two types of 2201 structure, denoted by 1 and 2, which are stacked along $\vec{c}$ either in a regular alternation to form a 1, 2 sequence with a periodicity of 24 Å, or in a less regular sequence to form defective intergrowths (i). Note that the EDS analyses have been performed selecting the different areas (m, 1 or i) and that, in the limit of the accuracy of the technique, no significant variation of the composition has been detected.

A platelet crystal ($0.16 \times 0.11 \times 0.02$ mm^3) has been selected and mounted on an Enraf-Nonius CAD4 diffractometer. A few weak satellite reflections could be detected with the diffractometer. So, the important Pb substitution rate does not involve the complete

disappearance of the modulation, but, according to TEM results, one can assume that the modulated structure is restricted to just a minor part of the crystal, and that the major part of it is not modulated any longer. No significant diffuse scattering could be observed by means of x-ray diffraction.

1543 and 919 independent reflections with $I > 3\sigma(I)$ were measured using Mo Kα radiation respectively for the modulated and non-modulated phase. The two sets of reflections were first corrected for Lorentz and polarization effects, and then absorption correction based on crystal morphology was applied.

The experimental data from the collections are summarized in table 1.

Table 1. Experimental data.

	BiPbCo (crystal A)	BiPbCo (crystal B)
Chemical formula	$Bi_{1.84}Pb_{0.16}Sr_{2.08}CoO_{5.85}$	$Bi_{1.2}Pb_{0.8}Sr_2Co_{1.02}O_{6.2}$
Crystal size (mm^3)	$0.400 \times 0.080 \times 0.024$	$0.160 \times 0.110 \times 0.020$
Cell parameters (Å)	$a = 5.453(2)$ $b = 5.426(2)$ $c = 23.43(1)$	$a = 5.3117(7)$ $b = 5.4232(6)$ $c = 23.590(2)$
T (K)	294	294
Modulation wavevector	$\vec{q}^{\star}[0, 0.245(2), 1]$	
Space group	$F2mm(0\beta1)00s$	$Pnan$
Z	4	4
Data collection	CAD4 diffractometer/STOE IPDS	CAD4
Wavelength (Å)	λ(Mo Kα) = 0.71073	λ(Mo Kα) = 0.71073
Registered space	**CAD4**: h: 0, 10; k: −10, 10; l: 0, 46; m: −2, 2 **IPDS**: h: 0, 4; k: −4, 5; l: 0, 23; m: −2, 2	h: −10, 10; k: 0, 10; l: 0, 47
No of measured reflections	**CAD4**: 13552 **IPDS**: 14048	2799
No of reflections with $I > 3\sigma(I)$	**CAD4**: 1040 **IPDS**: 503	919
Rho_{min}, Rho_{max} (e Å^{-3})	−4.0, 4.7	−5.3, 4.9
No of refinement parameters	86	74
R, wR ($hklm$)	0.048, 0.049	0.072, 0.064
R, wR ($hkl0$)	0.036, 0.046	
N_0	212	919
R, wR ($hkl1$)	0.048, 0.048	
N_1	471	
R, wR ($hkl2$)	0.062, 0.067	
N_2	357	

3. Structure refinement

3.1. The incommensurately modulated phase, $x = 0.16$

The incommensurate modulated Pb-doped structure has been refined using the 4D superspace formalism for modulated structures already described for the structure refinement of the corresponding lead-free phase [1]. The same symmetry as for the undoped compound was observed and thus the superspace group $F2mm(0\beta1)00s$ was assumed. The program JANA98 [3] has been used.

As in the previous study, two bismuth sites (Bi_1 and Bi_2) and two oxygen sites (OB_1 and OB_2) have been introduced. It is in fact not possible to describe all Bi and O atoms (OB) of [BiO] layers as a function of the internal phase parameter, with only one site. In order to describe the alternate occupation of the two sites, a harmonic occupation function has been introduced for Bi atoms and a crenel one for OB atoms. In this step, an important difference from the previously reported study should be pointed out. Fourier maps did not show any evidence for split OB sites along $\vec{x}$, and so only one fully occupied OB site has been introduced here. A crenel occupation function has also been refined for O atoms in [SrO] layers (OS) which reveals vacant sites around $x_4 = 0.25$.

Anisotropic atomic displacement parameters were taken for cations and isotropic ones for oxygen atoms. A thermal parameter modulation was refined for cations.

The global agreement factor is $R = 0.048$ with $R_0 = 0.036$ for the main reflections, $R_1 = 0.048$ and $R_2 = 0.061$ for the first- and second-order satellites, respectively. The refinement results for this phase are given in tables 2, 3, 4 and 5.

3.2. The non-modulated model for the highly doped phase, $x = 0.8$

This structure was also refined using the JANA program [3], neglecting the few satellite reflections of very weak intensity.

The modulated structures of the 2201-type compounds are consistent with an F centring of their average structure. In the present case, two sets of reflections can be distinguished in the data collection; the first one, of strong intensity, is also consistent with an F centring ($h+k = 2n$, $h+l = 2n$ and $k+l = 2n$), but the second one, of weaker intensity, significantly breaks the previous centring symmetry (386 reflections with $I > 3\sigma(I)$) leading to a primitive lattice. According to these observations, a preliminary model for cationic positions, within the F-lattice approximation, was derived assuming for BiO, SrO and CoO_2 layers the same type of sequence along $\vec{c}$ as in the related compounds. Then, the refinement was performed in the group $Pnan$, according to the observed reflection conditions ($0kl$, $k+l = 2n$; $h0l$, $h = 2n$; and $hk0$, $h+k = 2n$).

A first refinement in this group was carried out using the second data set. Then, it was carried out on the whole data set. At this stage, the global R-factor was still quite high. The observation of Fourier maps around each cationic site revealed a systematic asymmetric splitting of the atomic positions (figures 3 and 4). The electron density is characterized by a main and a secondary maximum, slightly displaced along $\vec{x}$ from each other. After the introduction of oxygen atoms, and even with a weaker contrast, a comparable observation could be made as regards the oxygen sites. In a first approximation, the ratio between the intensities of the two related maxima seemed to be roughly constant for all kinds of atom. At this stage, each site was split in the refinement and the relative occupancy of the doubled sites was refined. As the relative occupancies of each of the cationic double sites are always almost the same, a first interpretation consists in associating all predominantly occupied sites in a main configuration and all weakly occupied sites in a

Table 2. Positional (A_i, B_i) and occupational (A'_i, B'_i) Fourier parameters for the modulated doped phase (crystal A). The notation is the same as in [1]. The $0^\star$ were fixed during the refinement because they are not significant. The $0^\dagger$ were constrained by symmetry.

		$A_0(P_0)$	$A_1(A'_1)$	$B_1(B'_1)$	$A_2(A'_2)$	$B_2(B'_2)$
Bi_1	U_1	0.0087(3)	0.0067(6)	$0^\dagger$	$0^\dagger$	0.0032(6)
	U_2	$0^\dagger$	$0^\dagger$	−0.08187(5)	−0.01293(6)	$0^\dagger$
	U_3	0.18650(1)	0.0093(3)	$0^\dagger$	$0^\dagger$	0.00008(2)
	P	0.7704(9)	−0.4066(6)	$0^\dagger$	$0^\dagger$	0.2731(9)
Bi_2	U_1	$0^\star$	−0.0234(7)	$0^\dagger$	$0^\dagger$	−0.012(1)
	U_2	$0^\dagger$	$0^\dagger$	−0.1675(9)	0.0566(6)	$0^\dagger$
	U_3	0.1924(1)	0.0095(1)	$0^\dagger$	$0^\dagger$	0.0007(1)
	P	0.2307(5)	0.3269(9)	$0^\dagger$	$0^\dagger$	−0.211(1)
Sr	U_1	0.5	0.0031(8)	$0^\dagger$	$0^\dagger$	−0.003(1)
	U_2	$0^\dagger$	$0^\dagger$	−0.04816(9)	−0.0065(1)	$0^\dagger$
	U_3	0.07662(1)	0.01941(2)	$0^\dagger$	$0^\dagger$	−0.00186(3)
	P	0.971(1)	−0.003(2)	$0^\dagger$	$0^\dagger$	−0.046(1)
Co	U_1	$0^\star$	$0^\dagger$	$0^\dagger$	$0^\dagger$	0.004(1)
	U_2	$0^\dagger$	$0^\dagger$	$0^\dagger$	−0.0030(2)	$0^\dagger$
	U_3	$0^\dagger$	0.02807(5)	$0^\dagger$	$0^\dagger$	$0^\dagger$
OC	U_1	0.257(2)	$0^\dagger$	$0^\dagger$		
	U_2	0.2500	$0^\dagger$	$0^\dagger$		
	U_3	$0^\dagger$	0.0179(1)	0.0056(6)		
OS	U_1	0.026(2)	$0^\star$	$0^\dagger$		
	U_2	$0^\dagger$	$0^\dagger$	−0.0622(6)		
	U_3	0.0993(1)	0.0103(2)	$0^\dagger$		
	Δ, x_4	0.876(3)	0.75			
OB	U_1	0.1043(7)	−0.020(1)	$0^\star$		
	U_2	0.391(1)	−0.077(1)	−0.053(2)		
	U_3	0.1887(4)	0.0182(3)	−0.0035(6)		
	P	0.473(4)	−0.139(7)	0.611(7)		
OBs	U_1	0.217(3)				
	U_2	0.2500				
	U_3	0.1712(4)				
	Δ, x_4	0.101(2)	0.25			

secondary configuration. The two corresponding configurations cannot be explained by any twin relationship.

The main configuration is predominant, with an occupation around six times greater than that of the second one. This predominance implies that all the related parameters could be refined with a good accuracy. As regards the second configuration, the weight of oxygen atoms is very weak in the refinement, so their occupancy and position should be handled carefully. It is important to notice that the direction of the splitting corresponds to the modulation direction of the undoped compound.

Anisotropic atomic displacement parameters were taken for cations (except for the Co

Table 3. Thermal parameters (Å^2) for crystal A.

	U_{iso}	U_{11}	U_{22}	U_{33}
Bi_1	0.01681(6)	0.0233(1)	0.01788(9)	0.00921(9)
Bi_2	0.0186(1)	0.0102(3)	0.0216(2)	0.0239(3)
Sr	0.0129(1)	0.0093(2)	0.0112(2)	0.0183(2)
Co	0.0107(3)	0.0036(5)	0.0034(3)	0.0248(6)
OC	0.0171(8)			
OS	0.0196(7)			
OB	0.0229(9)			
OBs	0.023(2)			

Table 4. Sine and cosine first-order parameters for the modulated thermal parameters (Å^2) for crystal A. The $0^\star$ were fixed during the refinement because they are not significant. The $0^\dagger$ were constrained by symmetry.

		sin	cos
Bi_1	U_{11}	−0.0031(2)	$0^\dagger$
	U_{22}	0.0072(1)	$0^\dagger$
	U_{33}	−0.0052(1)	$0^\dagger$
	U_{12}	$0^\dagger$	0.0012(6)
	U_{13}	0.0154(7)	$0^\dagger$
	U_{23}	$0^\dagger$	0.0009(1)
Sr	U_{11}	0.0045(4)	$0^\dagger$
	U_{22}	0.0065(3)	$0^\dagger$
	U_{33}	0.0040(4)	$0^\dagger$
	U_{12}	$0^\dagger$	$0^\star$
	U_{13}	$0^\star$	$0^\dagger$
	U_{23}	$0^\dagger$	$0^\star$
Co	U_{11}	$0^\dagger$	$0^\dagger$
	U_{22}	$0^\dagger$	$0^\dagger$
	U_{33}	$0^\dagger$	$0^\dagger$
	U_{12}	$0^\dagger$	$0^\dagger$
	U_{13}	$0^\dagger$	$0^\dagger$
	U_{23}	$0^\dagger$	−0.0053(5)

atom of the second configuration which was taken as isotropic) and isotropic ones for oxygen. The final global agreement factor in $Pnan$ is $R = 0.071$. The agreement factor for the reflections respecting the F centring is $R = 0.059$ while it is $R = 0.099$ for the others. The refinement results for both configurations are given in tables 6, 7, 8 and 9.

4. Discussion

It has been shown that the substitution of lead for bismuth in the 2201 cobaltite phase involves important structural changes mainly concerning the modulation scheme. This clearly confirms that the origin of the modulation phenomena lies in the interactions within and between [BiO] layers. A main result of the present work is that the oxygen configuration of the [BiO] layers is mainly concerned by these structural changes.

An introduction of a small amount of lead in the 2201 modulated phase results in a

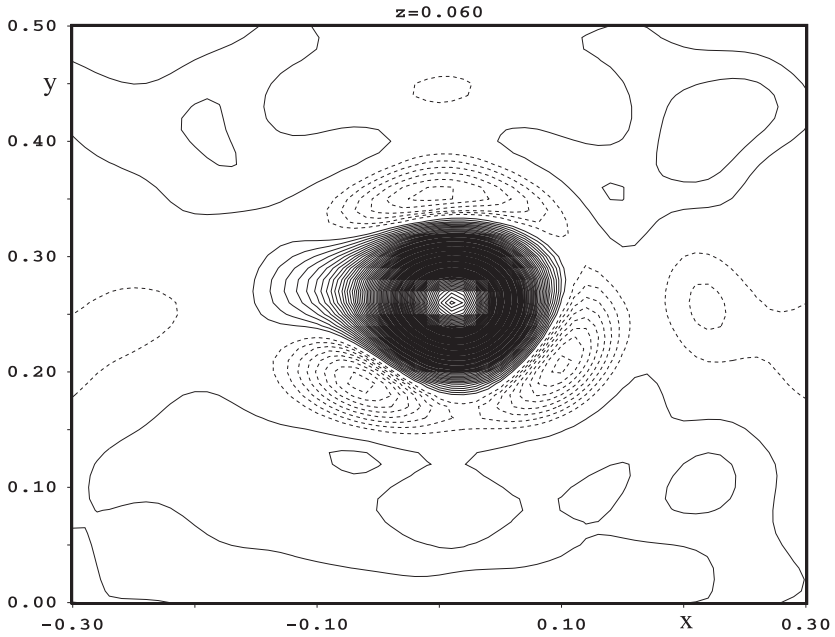

Figure 3. An x_1–x_2 section of the Fourier map around the Bi site ($z = 0.06$).

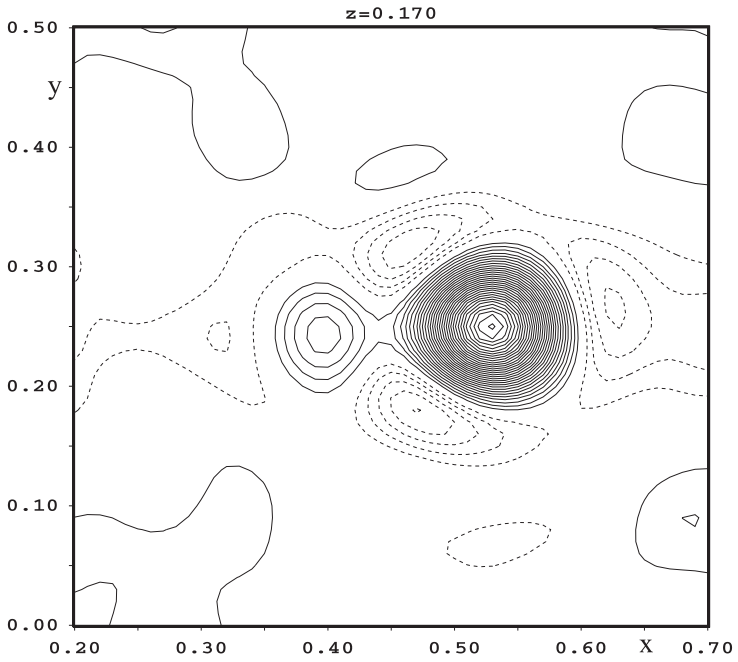

Figure 4. An x_1–x_2 section of the Fourier map around the Sr site ($z = 0.17$).

significant change of the oxygen configuration of the [BiO] layers. So, the study of this weakly doped phase allows a better understanding of the lead-free phase to be achieved thanks

Table 5. Bi–O distances and O–Bi–O angles, including also the electronic lone pair E of Bi^{3+}, in the modulated phase.

Bi(a)	OS(a)	OB(a)	OB(b)	E(a)	
OS(a)	**2.05**	2.95	3.04	2.62	
OB(a)	89	**2.16**	3.56	2.58	
OB(b)	92	110	**2.18**	2.24	
E(a)	146	123	87	**0.65**	
Bi(b)	OS(b)	OB(c)	OB(d)	OB(e)	E(b)
OS(b)	**2.06**	2.91	3.04	3.04	2.71
OB(c)	90	**2.06**	3.57	3.52	2.56
OB(d)	88	109	**2.32**	4.58	2.34
OB(e)	84	102	148	**2.45**	2.52
E(b)	145	125	82	87	**0.74**
Bi(c)	OS(c)	OB(f)	OB(g)	E(c)	
OS(c)	**2.04**	3.03	3.12	2.45	
OB(f)	93	**2.13**	3.71	2.21	
OB(g)	92	113	**2.30**	2.55	
E(c)	146	94	116	**0.48**	
Bi(d)	OBs(a)	OBs(b)	OB(h)	OB(i)	E(d)
OBs(a)	**2.06**	2.73	3.27	3.91	2.24
OBs(b)	79	**2.20**	2.66	4.35	2.59
OB(h)	149	71	**2.38**	3.52	2.46
OB(i)	116	133	92	**2.53**	2.32
E(d)	111	164	97	54	**0.40**

Table 6. Occupational and positional parameters for the first configuration of crystal B.

	O	*x*	*y*	*z*
Bi_1	0.626(6)	0.2637(1)	0.0119(2)	0.06122(1)
Sr_1	0.650(7)	0.2497(4)	0.5337(2)	0.17352(3)
Co_1	0.666(3)	0.25	0.0319(4)	0.25
OC_1	0.65(1)	0.498(1)	0.283(1)	0.2465(3)
OS_1	0.47(1)	0.235(2)	0.027(2)	0.1503(3)
OB_1	0.89(1)	0.349(1)	0.622(1)	0.0660(3)

Table 7. Occupational and positional parameters for the second configuration of crystal B.

	O	*x*	*y*	*z*
Bi_2	0.146(3)	0.2709(6)	−0.0917(9)	0.0636(1)
Sr_2	0.079(3)	0.241(4)	0.411(2)	0.1831(5)
Co_2	0.104(3)	0.25	−0.093(3)	0.25
OC_2	0.13(1)	0.513(2)	0.178(2)	0.261(1)
OS_2	0.28(1)	0.223(4)	−0.099(4)	0.1526(6)
OB_2	0.18(1)	0.297(5)	0.532(5)	0.078(1)

to the stabilization of just one configuration for the [BiO] layers. The modulated character of the undoped and weakly doped phases disappears with a larger Pb substitution rate.

Table 8. Thermal parameters (Å^2) for the first configuration of crystal B. The 0* were fixed during the refinement because they are not significant. The 0† were constrained by symmetry.

	U_{iso}	U_{11}	U_{22}	U_{33}	U_{12}	U_{13}	U_{23}
Bi_1	0.0088(1)	0.0142(4)	0.0061(1)	0.0062(1)	0*	−0.0010(1)	−0.0002(1)
Sr_1	0.0069(2)	0.0115(6)	0.0033(3)	0.0059(2)	0*	−0.0012(5)	−0.0033(3)
Co_1	0.0108(4)	0.0057(8)	0.0056(5)	0.0211(9)	0†	0.0016(7)	0†
OC_1	0.0059(8)						
OS_1	0.005(1)						
OB_1	0.023(1)						

Table 9. Thermal parameters (Å^2) for the second configuration of crystal B. The 0* were fixed during the refinement because they are not significant. The 0† were constrained by symmetry.

	U_{iso}	U_{11}	U_{22}	U_{33}	U_{12}	U_{13}	U_{23}
Bi_2	0.0194(6)	0.020(1)	0.008(1)	0.025(3)	−0.002(1)	0*	0*
Sr_2	0.0130(4)	0.006(3)	0.005(2)	0.027(2)	0*	0*	0.006(3)
Co_2	0.020(2)						
OC_2	0.07(6)						
OS_2	0.012(2)						
OB_2	0.026(5)						

4.1. The weakly doped modulated configuration

Except the oxygen configuration of the [BiO] layers, the modulated Pb-doped phase presents the same structural features as the lead-free phase already described [1]. The structure refinement also leads us to introduce a second site for Bi and OB atoms in the range $x_4 = [0.2–0.3]$. Bi_1 and OB_1 are present in approximately three consecutive cells out of four, defining what can be called a modulated zone (called M) in reference to the previous descriptions of related compounds. Indeed, the modulation is clearly visible in this zone, particularly along $\vec{c}$ (see figure 3 in reference [1]). In these zones, the displacements are close to those of the related 2212 cuprate or ferrite phases. The position of the $6s^2$ electronic lone pair Lp has also been calculated using the program PAIR [5, 6]. In the M zone, lone pairs are oriented towards the $\vec{a}$-direction: This uniform distribution of the orientation of the lone pairs differs from the usual scheme for the modulated structures of the cuprate phases. Between the M zones, Bi_2 and OB_2 appear in one cell involving a particular configuration with the electronic lone pair close to the Bi^{3+} ion ($d_{Bi-E} = 0.4$ Å). This zone is called intermediate (I). In consequence, in the modulation direction $\vec{b}$, we observe the same alternation of zones M and I as in the lead-free phase.

The most important difference with respect to the undoped phase is present in the M zone: the x-splitting introduced for the OB atom is no longer observed. The y-splitting is maintained because it allows a better description of the electron density. Consequently, the oxygen disorder disappears and only one configuration is stabilized in [BiO] layers. This configuration (figure 5) is similar to the 'honeycomb' one of the undoped phase with a symmetric arrangement of OB atoms around Bi.

The resulting configuration of the [BiO] layers is very different from the double chains characteristic for the related cuprate and ferrite structures. The Bi^{3+} environment in the honeycomb configuration is also different. It is characterized by three short Bi–OB distances in the $(\vec{a}, \vec{b})$ plane with O–Bi–O angles greater than 90° (table 5). A fourth short apical Bi–OS distance is also observed.

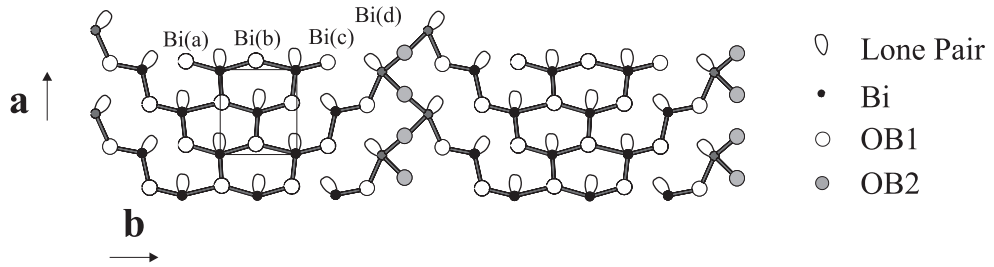

Figure 5. The [BiO] layer configuration in crystal A. Bi–O interatomic distances <2.6 Å are represented by solid lines. The average unit cell is represented by solid lines.

Bond valencies have been calculated using the model of Brown and Altermatt [7, 8]. Sr atoms are surrounded by seven or eight oxygen atoms according to the occupation of the OS site. The Co atom is in an octahedral configuration in the M zone, leading to a calculated bond valency of 2.5. In the I zone, the absence of OS involves a pyramidal configuration and thus a bond valency of 2.1.

4.2. The non-modulated phase

The highly Pb-doped compound is no longer modulated. Nevertheless, the main characteristics of the non-modulated structure are similar to those of the average structure of the modulated compound ($F2mm$ symmetry). The study of this non-modulated phase confirms the existence of a new configuration for [BiO] layers and thus the results previously obtained for modulated phases. The modulation is now replaced by a new disordered atomic sequence which can be described as the simultaneous presence of two different structural configurations compatible with a single symmetry group $Pnan$. The apparent split sites for practically all the atoms are the consequence of the artificial merging into one unit cell of these two configurations in the structural refinement. In fact, as indicated by TEM results, these configurations are characteristic for two types of coherent domain in the structure. This has been confirmed by high-resolution microscopy which has shown that this disorder probably results from various stacking sequences of both configurations along the $\vec{c}$-direction (see below). The predominant one, denoted as configuration 1, is characterized by an occupation around six times greater than that of the second one (configuration 2). The displacements from the ideal atomic positions corresponding to the $F2mm$ average structure and responsible for the symmetry reduction are not very important (<0.2 Å for configuration 1), but atoms are leaving these special positions to go to general ones, except the Co atom which is on a binary axis.

4.2.1. The main non-modulated configuration. This structure can still be interpreted as BiO–SrO–CoO_2–SrO–BiO slabs stacked in the $\vec{c}$-direction (figure 6). One observes an increase of the c-parameter from the modulated phase ($c = 23.41$ Å) to the non-modulated one ($c = 23.59$ Å). This can be explained, on one hand, by the increase of BiO–BiO interlayer distances and, on the other hand, by the absence of rotation of the CoO_6 octahedra around $\vec{a}$, involving a larger SrO–SrO interlayer distance in the slab.

The observation of [BiO] layers reveals, in the $\vec{b}$-direction (corresponding to the modulation direction of the undoped phase), a configuration similar to the previous so-called 'honeycomb' configuration of the modulated phases (figure 7) without the original splitting of the oxygen sites. Indeed, it is distorted by a lengthening in the $\vec{b}$-direction resulting in a less

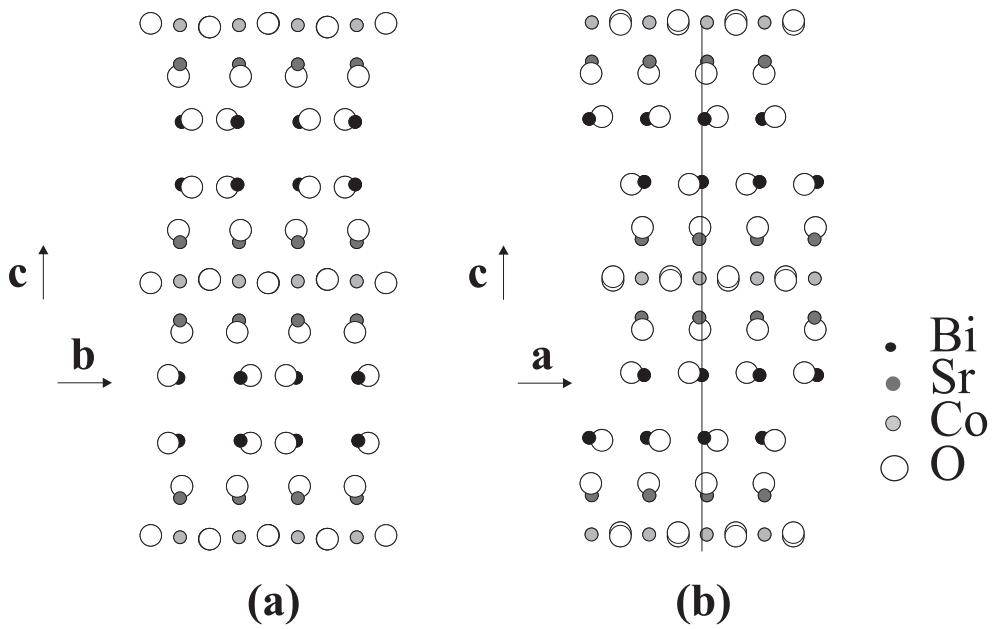

Figure 6. Projections of the structure of $Bi_{1.2}Pb_{0.8}Sr_2CoO_6$ in configuration 1 (a) along $\vec{a}$ and (b) along $\vec{b}$.

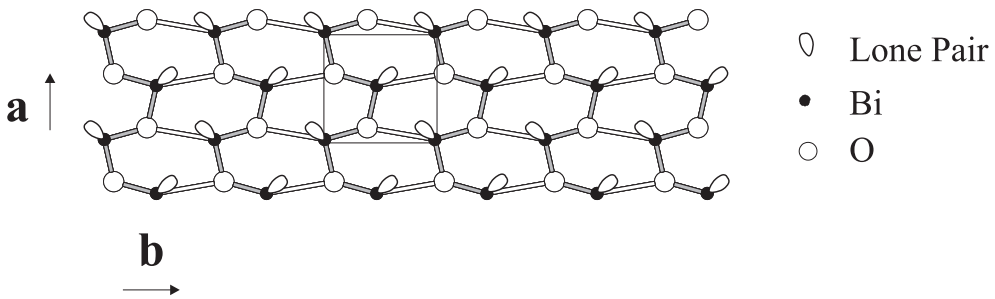

Figure 7. [BiO] layers for configuration 1 in crystal B. Interatomic Bi–O distances <2.2 Å are represented in grey and those <3.4 Å are represented in white. The average unit cell is indicated by solid lines.

symmetrical environment for Bi atoms. These atoms are surrounded, in the ($\vec{a}$, $\vec{b}$) plane, by only two OB atoms with short Bi–OB distances (table 10).

Table 10. Bi–O distances and O–Bi–O angles, including also the electronic lone pair E of Bi^{3+}, for the first configuration of crystal B.

Bi_1	OS_1	OB_1	OB_1	Lp_1
OS_1	**2.11**			
OB_1	90	**2.13**		
OB_1	90	93	**2.18**	
Lp_1	135	124	114	**0.82**

Lone-pair calculations lead to a reasonable value of 0.82 Å for the Bi–Lp distance. Indeed, lone pairs are not oriented along $\vec{a}$ as in the honeycomb modulated configuration, but are alternately oriented towards [110] and [1$\bar{1}$0] directions, in the opposite direction to the short Bi–O distances. This special lone-pair configuration and the consideration of the shorter Bi–O bonds allow us to describe [BiO] layers in terms of double chains very similar to the previously described BiO double chains of the ferrites and cuprates in their non-disordered regions. These double chains, characteristic for the cuprate or ferrite phases, are now infinite, not modulated and orthogonal to the direction of the modulation in 2201 cobaltite structures as deduced from the residual weak satellite reflections of our samples, or of the honeycomb orientation of the [BiO] layers.

The Co environment is very symmetrical with four short equatorial distances (1.9 Å) and two long apical distances (2.35 Å). The calculated bond valence is 2.65. The Sr atom is surrounded by nine oxygen atoms and the calculated bond valence is 2.05.

4.2.2. The secondary non-modulated configuration. The structural parameters describing configuration 2 are less reliable than the corresponding ones for the main configuration, owing to the weak occupation of the corresponding sites, especially for the oxygen atoms. Nevertheless, the same general features as for the previous configuration can be noticed.

The main difference from configuration 1 results from a higher value of the shift of the atoms from their 'symmetry site' of the parent $F2mm$ structure. As a consequence, two neighbouring BiO–SrO–CoO_2–SrO–BiO slabs are shifted from each other by around 1 Å (figure 8).

The honeycomb configuration along $\vec{b}$ of the [BiO] layers is confirmed by the projection on the ($\vec{a}$, $\vec{b}$) plane (figure 9), but the Bi environment is more regular and lone pairs are oriented along $\vec{a}$. The bismuth environment is now characterized by only one long and two short distances (table 11).

The existence of BiO double chains along $\vec{a}$ is also confirmed in this configuration.

Table 11. Bi–O distances and O–Bi–O angles, including also the electronic lone pair E of Bi^{3+}, in the second configuration of crystal B.

Bi_2	OB_2	OS_2	OB_2	Lp_2
OB_2	**2.02**			
OS_2	80	**2.11**		
OB_2	100	89	**2.45**	
Lp_2	131	147	95	**1.00**

5. High-resolution electron microscopy

These structural results for the non-modulated phase are confirmed by high-resolution microscopy observations. Indeed, the two types of contrast observed in the non-modulated areas of the crystal lead us to describe the structure as an intergrowth of two different configurations. In consequence, simulations have been done, using the Mac Tempas program, on the basis of the above structural results, in order to analyse the experimental images.

For a focus value close to −45 nm (figure 10(a)), the predominant contrast consists in double rows of bright dots, spaced by 12 Å and running perpendicularly to $\vec{c}$; they are correlated with the double [(Bi, Pb)O] layers. Within these layers, there are two possible different arrangements of the bright dots (see the relative positions of the black arrows): they are either facing

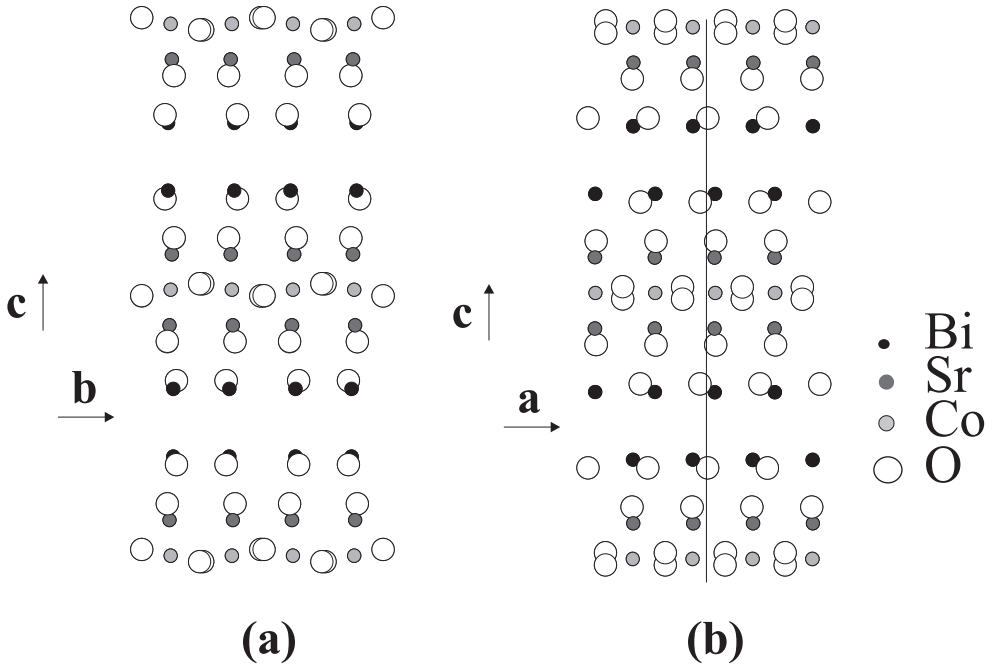

Figure 8. Projections of the structure of $Bi_{1.2}Pb_{0.8}Sr_2CoO_6$ in configuration 2 (a) along $\vec{a}$ and (b) along $\vec{b}$.

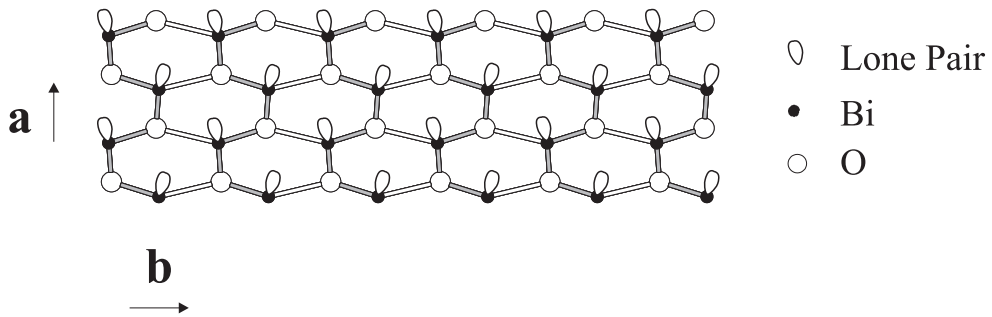

Figure 9. [BiO] layers for configuration 2. Interatomic Bi–O distances <2.7 Å are represented in grey and those <3.2 Å are represented in white.

each other or in staggered positions. Image calculations (figure 10(b)) show that staggered positions of the bright dots are only observed for the [010] orientation of configuration 2 ($[010]_2$), and so can be attributed to this configuration. Configuration 2 is indeed characterized by a shift between two neighbouring slabs. The other arrangement of the bright dots, i.e. aligned along $\vec{c}$, corresponds as well to the $[100]_1$ image as to the $[100]_2$ one.

The above contrast is especially visible in the thinner parts of the samples where distortions and domain superimpositions which could prevent an accurate interpretation in the thicker part are minimum. However, the difference between the two [010] configurations is also observed in the thicker part, especially for focus values close to -10 and -30 nm. An example is given in figure 11. The contrast at the level of the double [(Bi, Pb)O] layers is dark in configuration

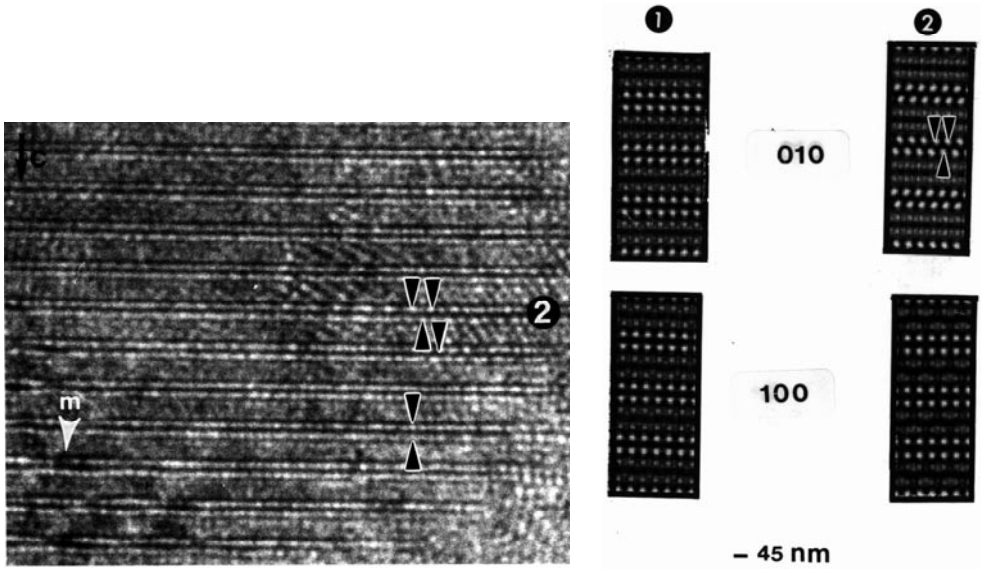

(a) (b)

Figure 10. (a) A HREM image recorded for a focus value close to −45 nm. The different positions of the bright dots within a double [(Bi, Pb)O] layer are indicated by dark arrows. (b) Calculated images for configurations 1 and 2 and for two orientations [100] and [010], equivalent directions of the pseudotetragonal subcell. (The crystal thickness is assumed to be close to 3 nm.)

2 (white arrows) and bright in configuration 1. The theoretical images calculated for crystal thicknesses varying from 15 to 90 Å are shown in figure 11. This contrast is the one which allows the easiest interpretation of the images.

From the above identification of the contrast, configuration 1 is, by far, the most frequently observed, over large areas of the particles. A very frequent event is intergrowth of the two configurations. The stacking sequences are sometimes irregular, as in the area denoted by i (figure 2(a)), but one often observes the alternation of one half-slice of structure 1 with one or two half-slices of configuration 2, forming polytypes (1, 2) and (1, 2, 2) respectively. One example is given in figure 12. The c-parameter of the (1, 2) member is $c_{12} = 24$ Å and that of (1, 2, 2) is $c_{122} = 72$ Å.

The resulting ED patterns are the superimpositions of all the polytypes. Moreover, a detailed analysis of the images shows that a twinning effect also exists, with [100] and [010] domains, which results from the pseudotetragonal character of the subcell. The coexistence of these configurations, and their more or less random distribution along $\vec{c}$, explain the local lowering of the symmetry observed in the ED patterns.

6. Conclusions

The present structural study of the different $Bi_{2-x}Pb_xSr_2CoO_{6-y}$ phases produces two main new results.

First, [BiO] layers are now characterized by a new configuration which is compared with the known ones for the related 2201 or 2212 cuprates and ferrites. This 'honeycomb' configuration is clearly observed in the doped 2201 cobaltite compounds, modulated or not. This configuration was only presumed as a possible hypothesis in the previous description

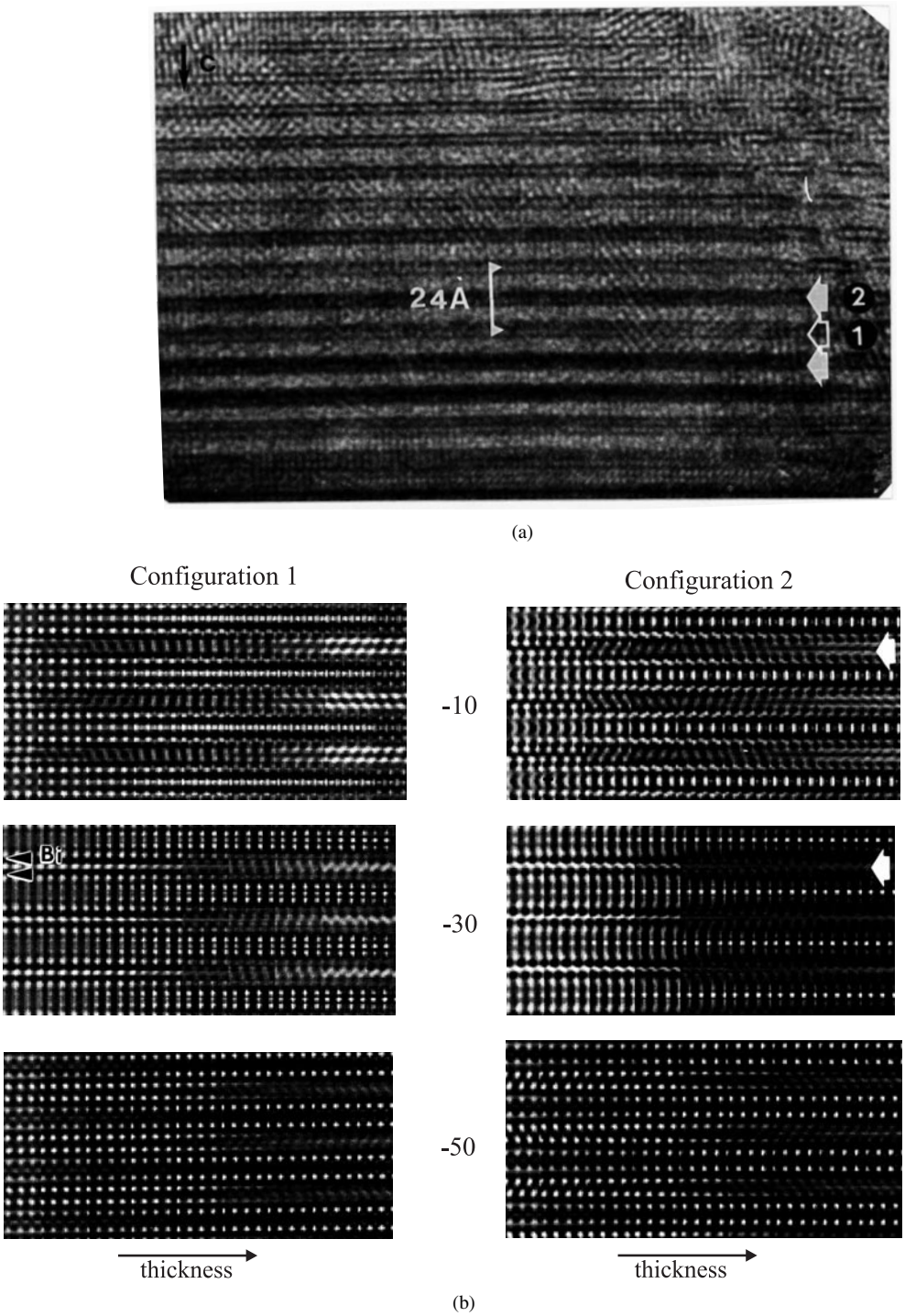

Figure 11. (a) A HREM image showing the variations of contrast at the level of a half-slice. The dark (white) arrows and less dark (open) arrows layers alternate along $\vec{c}$. (b) Calculated images for configurations 1 and 2, with varying thickness (horizontal) and focus (vertical).

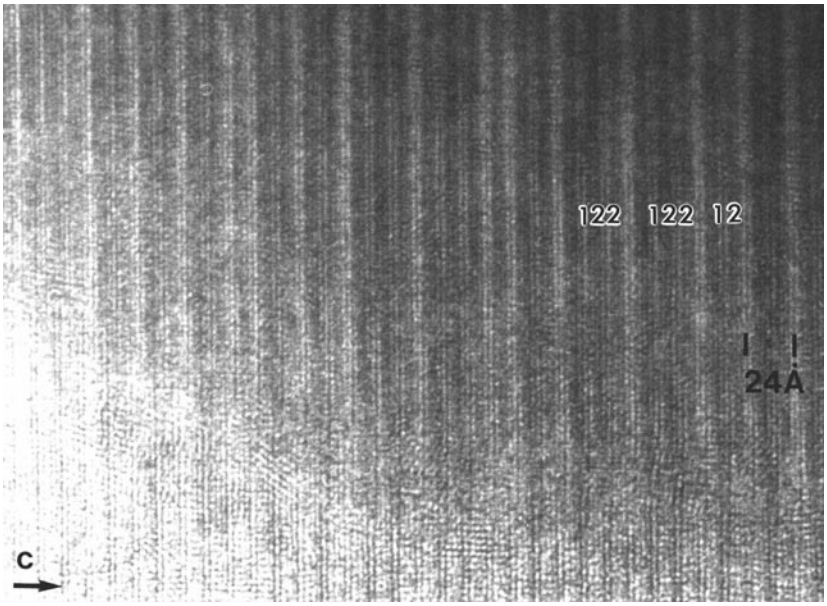

Figure 12. A high-resolution image of the non-modulated phase; observation of polytypes (1, 2) or (1, 2, 2).

of the modulated lead-free 2201 cobaltite. It is characterized by a homogeneous distribution of Bi atoms in the ($\vec{a}$, $\vec{b}$) plane and by O–Bi–O angles greater than 90°. It leads to a new Bi^{3+} environment. In this configuration, lone pairs are oriented roughly perpendicularly to the modulation direction.

The same structural features can be seen in the non-modulated compound which can be described as a stacking along $\vec{c}$ of two configurations in ordered mode forming polytypes or in a disordered mode. Indeed, in this phase, the orientation of lone pairs in the [110] and [1$\bar{1}$0] directions now indicates the existence of double chains close to those observed in cuprates but perpendicular to the modulation direction of cobaltites. Nevertheless, these double chains only result from the asymmetric positioning of the oxygen atoms, leading to systematically longer or shorter Bi–O distances, and not from the Bi positions themselves. In fact, Bi atoms are almost equidistant in the ($\vec{a}$, $\vec{b}$) plane, while in related cuprates or ferrites, they were also characterized by systematically longer and shorter Bi–Bi distances. One can also notice the relatively high R-value for this non-modulated phase. This can be explained by the important stacking disorder observed in this structure and by the superimposition of microdomains along $\vec{c}$. One cannot *a priori* exclude the occurrence of the double-chain configuration for the lead-free phase. In fact, preliminary results concerning another cobaltite phase with a double modulation seem to indicate that this configuration is also possible.

Secondly, the modulation scheme is quite different from the corresponding well known one for cuprates and ferrites. It is not based on the internal modulation of BiO double chains, but rather on the mutual interaction between parallel infinite and non-modulated double chains. The apparent analogy between the two types of modulated structure rather results from a pseudosymmetry phenomenon, clearly evidenced in a first observation of the corresponding diffraction patterns, but the real discrepancy is also indicated by the significant difference between the respective irrational components of the modulation vectors (0.21 for cuprates versus 0.24 for cobaltites) and by the different evolution towards the commensurate value

as a function of lead substitution (0.2 for cuprates versus 0.25 for cobaltites). Unlike the ferrite phases, the cobaltite ones seem inappropriate for improving the description of the superconductor cuprate phases.

Acknowledgment

The authors wish to acknowledge Professor M Evain for the collection of data for crystal A on a STOE IPDS.

References

[1] Jakubowicz N, Grebille D, Leligny H and Evain M 1999 *J. Phys.: Condens. Matter* **11** 3997
[2] Tarascon J M, LePage Y, McKinnon W R, Ramesh R, Eibschutz M, Tselepis E, Wang E and Hull G W 1990 *Physica* C **167** 20
[3] Petříček V 1998 *Crystallographic Computing System Jana98* Institute of Physics, Academy of Sciences of the Czech Republic, Prague
[4] Tarascon J M, Miceli P F, Barboux P, Hwang D M, Hull G W, Giroud M, Greene L H, LePage Y, McKinnon W R, Tselepis E, Pleizier G, Eibschutz M, Neumann D A and Rhyne J J 1989 *Phys. Rev.* B **39** 11 587
[5] Le Bellac D, Kiat J M and Garnier P 1995 *J. Solid State Chem.* **114** 459
[6] Jakubowicz N, Pérez O, Grebille D and Leligny H 1998 *J. Solid State Chem.* **139** 194
[7] Brown I D and Altermatt D 1985 *Acta Crystallogr.* B **41** 244
[8] Brese N E and O'Keefe M 1991 *Acta Crystallogr.* B **47** 192
[9] Janssen T, Janner A, Looijjenga-Vos A and De Wolff P 1992 *International Tables for Crystallography* (Dordrecht: Kluwer)